Excitation Energy Dependent Charge Separation at Hole- Transporting Dye/TiO 2 Hetero Interface

DATASET *in* THE JOURNAL OF PHYSICAL CHEMISTRY C · AUGUST 2012

Impact Factor: 4.77 · DOI: 10.1021/jp302187w

7 AUTHORS, INCLUDING:

Eva L Unger
Lund University
20 PUBLICATIONS **386** CITATIONS
SEE PROFILE

Anders Hagfeldt
École Polytechnique Fédérale de Lausanne
388 PUBLICATIONS **31,699** CITATIONS
SEE PROFILE

Gerrit Boschloo
Uppsala University
196 PUBLICATIONS **14,000** CITATIONS
SEE PROFILE

THE JOURNAL OF PHYSICAL CHEMISTRY C

Article

pubs.acs.org/JPCC

Excitation Energy Dependent Charge Separation at Hole-Transporting Dye/TiO_2 Hetero Interface

Eva L. Unger,[†] Tomas Edvinsson,[†] Joseph D. Roy-Mayhew,[‡] Håkan Rensmo,[§] Anders Hagfeldt,[†] Erik M. J. Johansson,[†] and Gerrit Boschloo*[,†]

[†]Department of Chemistry-Ångström Laboratory, Uppsala University, Box 523, SE 751 20 Uppsala, Sweden

[‡]Department of Chemical and Biological Engineering, Princeton University, United States

[§]Department of Physics and Astronomy, Molecular and Condensed Matter Physics, Uppsala University, Box 516, SE 751 20 Uppsala, Sweden

Supporting Information

ABSTRACT: Interfacial charge separation in hybrid solar cells depends on both the energetic alignment and electronic coupling between the inorganic and organic semiconducting materials at the hetero interface. In the present work, bilayer solar cells comprising the small molecular semiconducting dye TDCV-TPA (tris-(thienylene-vinylene)-triphenylamine) and dense titanium dioxide (TiO_2) films were investigated. The internal quantum efficiency and degree of photoluminescence quenching were found to be excitation energy dependent. The molecular interaction and interfacial energy level alignment was investigated using a combination of UV−vis and photoelectron spectroscopy (PES). Stationary and time-dependent density functional theory calculations were used to assign and distinguish between different experimentally determined molecular energy levels (PES) and electronic transitions (UV−vis). Photoelectron spectroscopy results suggest surface induced interactions of TDCV-TPA with TiO_2 involving the peripheral CN-groups of the molecule which would imply a favorable electronic coupling for photoinduced interfacial charge transfer. In an energy level diagram distinguishing between the different electronic transitions in the molecule, the differences in the thermodynamic driving force for electron injection from the excited states were found small. Therefore, it is suggested that the observed higher internal quantum efficiency at shorter wavelength can be rationalized by a more favorable driving force for the regeneration of holes created at the hetero interface at higher excitation energy.

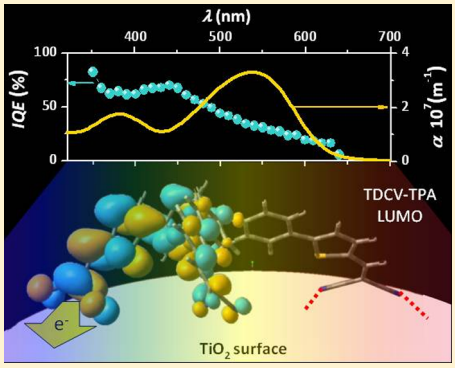

INTRODUCTION

Hybrid solar cells (HSCs), dye sensitized solar cells (DSCs), and organic solar cells (OSCs) have the potential to become flexible, lightweight and low-cost solar energy conversion devices.[1−4] Several motivations exist for conducting research on HSC devices: first, the costly C_{60} derivates in OSC can be replaced by low-cost inorganic semiconductors which often also have a higher electron affinity. Second, inorganic semiconductors can be synthesized with well-defined nanoscale morphologies[5] which can be beneficial to optimize exciton harvesting in the devices. However, when comparing HSC to OSC devices, the hybrid devices are often found to yield lower power conversion efficiencies due to a lower charge separation efficiency at organic/inorganic hetero interfaces. Understanding the fundamental physical processes determining the conversion of absorbed photons into separated charge carriers at hetero interfaces is therefore of crucial importance to improve power conversion efficiencies of HSCs.

In HSCs, using wide-band-gap inorganic semiconductors such as titanium dioxide (TiO_2) and bulk organic absorbers, light is absorbed predominantly in the organic component. The thickness of the organic layer and its absorption coefficient determine the light harvesting efficiency (LHE) of the device. Light absorption leads to the formation of excitons, which can contribute to the photocurrent if generated within the exciton diffusion length, L_{ED}, from a charge separating interface.[6,7] The exciton diffusion efficiency, η_{ED}, describes the efficiency of this process.

The charge separation process in HSC is related both to interfacial charge transfer processes discussed in DSC research[8,9] and to charge separation in OSCs.[10] Exciton dissociation is initiated by an interfacial photoinduced electron transfer step from the excited state of the light absorbing component to the electron acceptor, denoted by the charge-transfer efficiency, η_{CT}.[11] In the type of HSC investigated herein, the inorganic n-type semiconductor TiO_2 acts as electron acceptor and a small molecular semiconductor is used for light harvesting. Following interfacial electron transfer, a hole is created in the organic component. In DSCs, the efficiency of regeneration of such holes (oxidized dye

Received: March 6, 2012
Revised: August 8, 2012
Published: August 22, 2012

molecules) created at the charge separating interface by means of reduction by the reduced form of a redox couple is denoted as the regeneration efficiency, η_{reg}. The latter is a function of the thermodynamic driving force for electron transfer from the redox-couple or solid state hole conductor to the oxidized sensitizer.[12] In OSCs, however, the charge-separation efficiency is determined by the separation efficiency of interfacial geminate electron−hole pairs that exert a coulomb force on each other.[10] HSC is also expected to be limited by the geminate separation efficiency, η_{GS}, of such electron−hole pairs.[13] The effect of nongeminate recombination processes is included in the charge collection efficiency η_{CC}.

The external quantum efficiency for photocurrent generation, EQE, is the product of all these consecutive processes (see Figure 1):

$$EQE = LHE \times \eta_{ED} \times \eta_{CT} \times \eta_{GS} \times \eta_{CC} \quad (1)$$

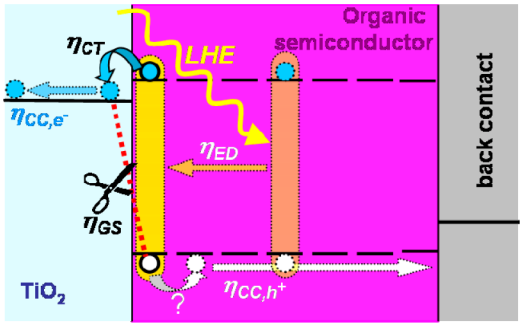

Figure 1. External quantum efficiency (EQE) determining steps in hybrid solar cells. After light harvesting (LHE) and exciton diffusion (η_{ED}), the device performance is determined by the interfacial charge separation efficiency, determined by the charge transfer (η_{CT}) and geminate separation (η_{GS}) efficiency.

In a previous study, we investigated HSCs comprising the small-molecular semiconducting dye TDCV-TPA as a dye-multilayer on dense titanium dioxide (TiO_2) substrates.[11] The HSC devices achieved power conversion efficiencies comparable to hybrid solar cells with similar architecture,[14−18] but considerably lower than that of OSCs with the same dye using C_{60} as electron acceptor.[19,20] The internal quantum efficiency (IQE) at the HSC interface was found to be less than unity and wavelength dependent. The interfacial energetic alignment and thus the driving forces for interfacial charge transfer were estimated from electrochemical measurements carried out in solution. This does not necessarily reflect the energetic alignment at the hybrid interface in a solid state device correctly.[21,22]

In this study, we will investigate this wavelength-dependent IQE further. An excitation energy dependent IQE can indicate "hot" electron injection from higher excited states.[23,24] According to the model proposed by Gerischer et al.,[9] the interfacial charge transfer rate k_{ct} is proportional to the overlap of the molecular levels in the excited state of the electron donating species $W_{D^*}(E)$ and the density of (unoccupied) states $DOS_{uo,A}(E)$ in the electron accepting wide-band-gap semiconductor:[8]

$$k_{ct}(E) \propto \int \kappa(E)\, DOS_{uo,A}(E)\, W_{D^*}(E)\, dE \quad (2)$$

where the transfer frequency $\kappa(E)$ is proportional to the electronic coupling V_{DA}^2 between the electron donor, D, and acceptor, A.

To derive a detailed energy level diagram depicting the energy distribution and differentiating between the different electronic transitions in the molecule, we will combine experimental data acquired from photoelectron (PES) and UV−visible spectroscopy on dye layers in different thickness domains. Theoretical results from DFT-calculations are used to distinguish between different HOMO energy levels measured in PES and to assign UV−vis bands to electronic transitions between specific molecular orbitals. PES has the advantage that the energy levels alignment of the dye at the hetero interface can be investigated in solid state and with respect to a common energy level. This way, changes in the interfacial energy level alignment due to the specific interaction of the components such as molecular band bending due to Fermi level alignment, charge transfer, and effects of molecular orientation can be evaluated.[21,25−31]

EXPERIMENTAL SECTION

The dye [tris(dicyano-vinyl-2-thienyl)phenyl]amine, TDCV-TPA (structure shown in the inset of Figure 2), was purchased

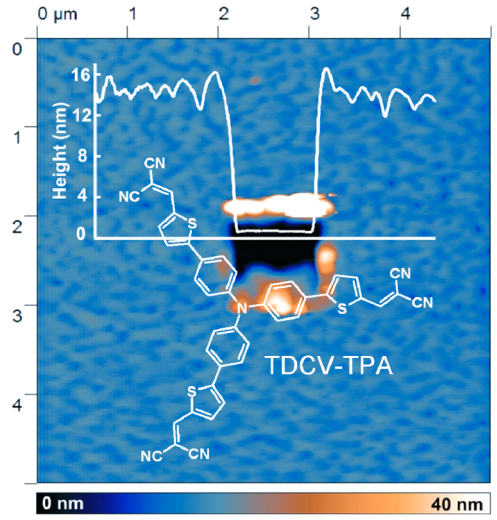

Figure 2. Atomic force microscope image of TDCV-TPA sample on mica with an average thickness of 13.1 ± 0.1 nm. Hard force contact mode was used to remove the dye from the image's center. Insets: line profile, in which *x*-axis represents the scan path and chemical structure of TDCV-TPA.

from Aldrich and used as received. Dye layers with varying thicknesses from submonolayer to multilayer were prepared by spin-coating dye solutions in dichloromethane (Aldrich) with concentrations varying from 0.05 to 10 mM at 4000 rpm for 30 s (Chemat Technology KW-4A spin-coater). Bilayer solar cell devices were fabricated using spray-pyrolyzed TiO_2 on conducting fluorine doped tin oxide (F:SnO_2) contacted with poly(3,4-ethylenedioxythiophene)/poly(styrenesulfonate) (PEDOT:PSS, Aldrich) and graphite powder (Aldrich) as described previously.[11] For optical characterization, thin layers of TiO_2 were prepared by spray pyrolysis from a ∼0.04 M titanium(di-isopropoxyl)(acetylacetonato) precursor solution in ethanol. The glass substrates were half masked with glass sheets during the deposition to allow for reference measurements to be performed on the dye on glass. The resulting TiO_2

dx.doi.org/10.1021/jp302187w | J. Phys. Chem. C 2012, 116, 21148−21156

films were optically thin and did not give rise to interference effects.

Absorption spectra of solid TDCV-TPA films and the dye dispersed in a solid poly(methylmethacrylate) (PMMA) matrix (1 μmol/g) were measured in a Cary5000 spectrometer. Photoluminescence (PL) excitation and emission spectra were recorded on a Fluorolog Jobin Yvon spectrofluorometer. Measurements were carried out at an angle of approximately 30° relative to the excitation beam. The photoluminescence quenching of TDCV-TPA was determined by comparing the PL_S on TiO_2 with the signal compared to glass substrate PL_{ref} corrected for the relative difference in the number of absorbed photons.

The thickness of the TDCV-TPA layers was determined by UV−vis spectroscopy using an absorption coefficient determined from correlating UV−vis spectra to thickness determined from atomic force microscopy (AFM) profile measurements. Measurements were carried out using contact-mode AFM on a MultiMode/Digital Nanoscope IIIa system (Veeco Instruments) using NPS-type tips.

The PES measurements were performed using synchrotron light at BL I411 at the Swedish National Laboratory MAX in Lund.[32,33] The takeoff angle used was 70°, and the angle between polarization and photoelectron direction was 0°. The spectrum of the TiO_2 sample without dye molecules was energy calibrated by setting the Fermi level to zero binding energy. The spectra for the samples with dye layers on the TiO_2 were energy calibrated by setting the titanium levels to the same binding energy as the uncoated TiO_2 sample, thereby following relative binding energies differences between the molecular layers and the TiO_2 substrate. The N1-NEXAFS spectra were recorded by detection of secondary electrons in the partial yield mode. The photon energy scale was calibrated by using photoelectron spectra excited by first and second order light.

DFT calculations were performed at a B3LYP/6-31+G(d) level using the Gaussian 09 quantum chemical package. Time dependent DFT and linear response frequency calculations were used to obtain the UV−vis spectra. To evaluate the shift in the absorption spectrum for TDCV-TPA in PMMA compared to solid films, a self-consistent reaction field (SCRF) solvent model with a polarizable continuum model (PCM) and the dielectric constant corresponding to PMMA was used. To estimate changes in energy due to the interaction of TDCV-TPA with TiO_2, the interaction energy of a single peripheral CN-group with a small section of an anatase crystal was calculated.

RESULTS

Dye Layer Thickness. In this study, the optical and electronic properties of the small molecular semiconductor TDCV-TPA (inset in Figure 2) films deposited on TiO_2 substrates were investigated. The dye layer thickness, d, for each sample was determined from the sample absorbance. For this, the absorption coefficient, α, of TDCV-TPA was determined by relating the absorbance, A, of TDCV-TPA samples on glass or mica substrates with d determined by AFM. Figure 2 shows the AFM image of a ~13 nm thick TDCV-TPA layer on mica. An area of ~1 μm^2 is visible in the center where the dye was removed by performing high force contact mode AFM.[34]

Subsequently, a low force contact mode AFM scan was taken in which the scan window was increased to 5 μm by 5 μm and the scan direction was shifted by 90°. The surface of the dye film consists of domains on the order of 100 nm in diameter. The height profile (inset in Figure 2) shows the ~2 nm roughness of the dye layer as well as the atomically smooth mica surface. The sample absorbances for dye layers d were related to their thicknesses to give $\alpha_{520nm} = 3.22 \times 10^7\ m^{-1}$ which is similar to the value determined using profilometry, reported elsewhere.[35] The entire spectrum of the absorption coefficient of TDCV-TPA is shown in Figure 3a.

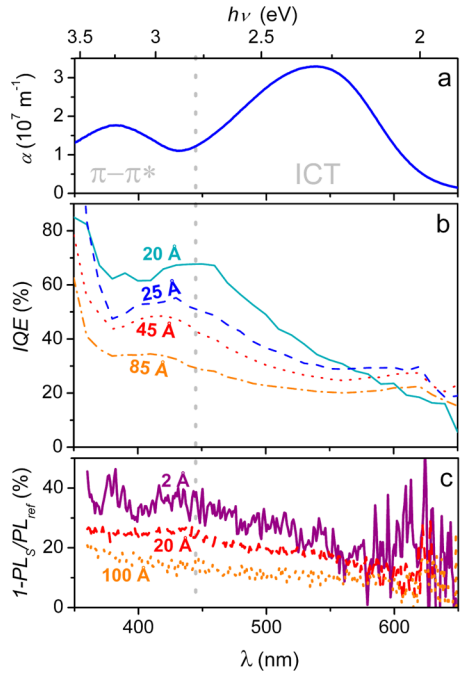

Figure 3. (a) Absorption coefficient α of TDCV-TPA. (b) Internal quantum efficiency (IQE) of bilayer hybrid solar cell devices of TDCV-TPA and TiO_2 (dye layer thickness d indicated in Figure). (c) Photoluminescence quenching of the excitation spectra of TDCV-TPA on TiO_2 with respect to a nonquenching glass substrate in dependency of wavelength for different dye layer thickness (d indicated in Figure).

IQE and PL-Quenching. The interfacial charge separation efficiency was examined both from the spectral response of the internal quantum efficiency for photocurrent generation, IQE (Figure 3b), and the wavelength-dependent PL-quenching of TDCV-TPA evaluated from PL-excitation spectra (Figure 3c). Only relatively thin dye layers, below 80 Å, were analyzed to avoid limitations arising from the limited exciton diffusion length (~ 65 Å)[35] and hole transport in TDCV-TPA.

The IQE was derived from the measured EQE and the LHE of the bilayer solar cell samples comprising TDCV-TPA with various d on spray-pyrolyzed TiO_2.[35] For small d, the η_{CT} and η_{GS} reflected in the IQE of the solar cell devices:

$$\eta_{CT}\eta_{GS} \propto \mathrm{IQE} = (1 - R)\frac{\mathrm{EQE}}{\mathrm{LHE}} \quad (3)$$

where R is taken as the reflectance measured for a TiO_2 coated FTO substrate. A strong wavelength dependence is observed, where the $\pi \rightarrow \pi^*$ transition yields up to 2 times larger IQE than the ICT transition.

The photoluminescence quenching was determined from the ratio between the excitation spectrum of TDCV-TPA films on a thin spray-pyrolyzed TiO_2 films, PL_S, and the excitation spectra of the dye on a nonquenching glass substrates, PL_{ref}, detecting

dx.doi.org/10.1021/jp302187w | J. Phys. Chem. C 2012, 116, 21148−21156

the photoluminescence at 710 nm. A plot of $1 - PL_S/PL_{ref}$ as a function of excitation energy is shown in Figure 3c.

For a ~20 Å thick TDCV-TPA film on titania the PL of the $\pi \rightarrow \pi^*$ transition is quenched by 25%, while the PL of ICT transition is quenched less (15%). Similarly, for a ~20 Å thick TDCV-TPA film in a solar cell configuration, the IQE for the $\pi \rightarrow \pi^*$ is higher than that for the ICT transition (65% and 30%, respectively). Thus, both experiments clearly indicate wavelength-dependent interfacial charge separation yields.

Photoelectron Spectroscopy. Photoelectron spectroscopy, PES, using synchrotron radiation was carried out to investigate the interface between the organic compound TDCV-TPA and the inorganic semiconductor TiO_2. The measurements were carried out on films of varying d deposited on dense layers of TiO_2 on FTO samples. The largest possible diameter of TDCV-TPA was estimated to be 28 Å from the molecular structure shown in Figure 2. Dye layers in the order of 1 Å are assumed to not entirely cover the TiO_2 surface and are therefore referred to as submonolayers. Dye layers in the order of tens of Å will presumably form mono- to bilayers on the titanium dioxide surface while dye layers in the order of 100 Å will form dye multilayers. As PES is a very surface-sensitive method, spectra measured for dye-multilayers should reflect on the properties of the dye molecules not in contact with the TiO_2 surface, while for submonolayers the effect of the substrate on the electronic properties of the dye will be visible.

In Figure 4a, the valence photoelectron spectra for the TDCV-TPA layers are compared for three different thickness

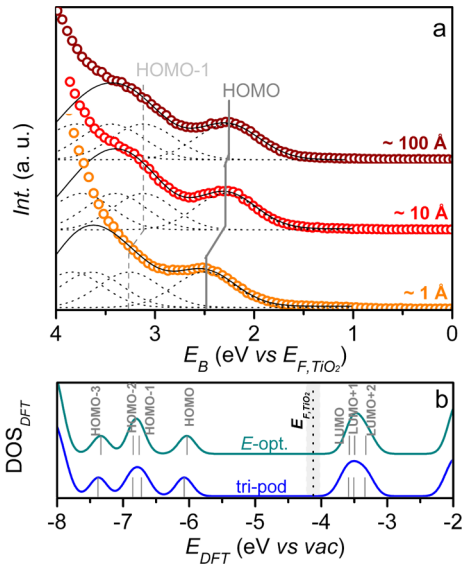

Figure 4. (a) Photoelectron spectroscopy valence spectra of dye layers with varying thicknesses on TiO_2 for different dye layer thicknesses measured with a photon energy of 100 eV. The values were are represented in binding energy E_B with respect to the Fermi level in uncoated TiO_2, E_{F,TiO_2}. (b) DOS of the highest occupied molecular orbitals (HOMOs) determined from DFT calculations.

regimes (indicated in figure). The valence photoelectron spectra were measured with respect to the Fermi level E_F in TiO_2. With respect to thicker dye layers, the HOMO for a dye layer in the order of 1 Å (submonolayer) is shifted toward higher binding energy by about 0.25 eV from 2.27 to 2.52 eV. The energy for HOMO levels of the TDCV-TPA molecules closest to the TiO_2 surface is lower in comparison to molecules in the bulk of the dye layer.

Theoretically calculated density of states (DOS) of the highest occupied molecular orbitals for an energy optimized TDCV-TPA (see Figure 7a) and a tripod-conformer (Figure 7b) are shown in Figure 4b. The approximate position of the E_F of TiO_2 is indicated in Figure 4b using an E_F of −0.50 V vs NHE as determined for spray-pyrolyzed TiO_2,[35] which corresponds to ~4.1 eV vs vacuum.[12] The theoretical values for the three highest molecular orbitals were used as a point of reference to fit the experimental PES data with Gaussians (Figure 4a). Fits made to the three lower HOMO levels are obscured by the onset of the TiO_2 valence band. The Gaussian fits are included in Figure 4a. The individual Gaussians are indicated with dashed lines and the resulting sum of the 4 lowest HOMO-levels is included as a solid line.

Previously, we have observed that triphenylamine-based molecules without the thiophene and cyano groups exhibit the opposite behavior: the HOMO level for the thin molecular layers shifted toward lower binding energies for submonolayers in comparison to the levels measured for thicker dye layers which represent molecules further away from the TiO_2 interfaces.[30] The reason for this shift was suggested to be caused by electron transfer from the molecules into the TiO_2, resulting in a shift of the energy levels in the molecular layers closest to the TiO_2 surface. To better understand the effects observed here, we investigated the S2p and N1s, as shown in Figure 5.

Structurally, the dye TDCV-TPA is rather similar to other triphenylamine dyes employed as sensitizer dyes in DSC that have been previously investigated with PES.[36,37] These dyes also consist of a triphenyl amine donor unit, linker units often containing thiophene-moieties, and anchor groups which often consist of a cyano-acrylic acid unit. Instead of a linear donor-linker-acceptor architecture, the dye investigated herein consists of three dicyano-vinyl-thiophenyl-branches symmetrically attached to the central triphenylamine unit. The photoelectron spectroscopy signals of the triphenylamine-nitrogen ($N1s_{TPA}$), thiophene-sulfur (S2p), and the cyano-nitrogen ($N1s_{CN}$) for TDCV-TPA are therefore expected to show similarities to, for example, the dye D5L0A1.[38,39]

Figure 5 shows the S2p (a) and N1s (b) spectra of dye layers of various d on TiO_2. Such S2p spectra always consists of contributions from $S2p_{1/2}$ and $S2p_{3/2}$, with the intensity ratio 1:2 and an energy split of about 1.2 eV, due to spin−orbit splitting. For the three samples, we observe a single spin orbit split doublet. The individual peaks can be fit with single Gaussian distributions, but for the submonolayer the distribution appears broadened. Comparing the binding energy of the S2p peaks in the different samples, we observe a clear shift toward lower binding energy for the thicker samples. The shift is similar to the shift we observed in the valence spectra of the samples (Figure 4a).

In the N1s spectra, we observe two features at about 403 and 401 eV. The signal around 403 eV we assign to the central triphenylamine-nitrogen atoms ($N1s_{TPA}$) and the signal around 401 eV to the CN-nitrogen atoms ($N1s_{CN}$) by comparison to previous measured dye molecules with similar molecular structures.[38,39] The large signal around 401 eV is broad and asymmetric. It may be fit with two Gaussians with an approximate ratio of 1:1. The reason for the appearance of two $N1s_{CN}$ peaks can be caused by dye−surface interactions, dye−dye interactions, and maybe slight differences in the

dx.doi.org/10.1021/jp302187w | J. Phys. Chem. C 2012, 116, 21148−21156

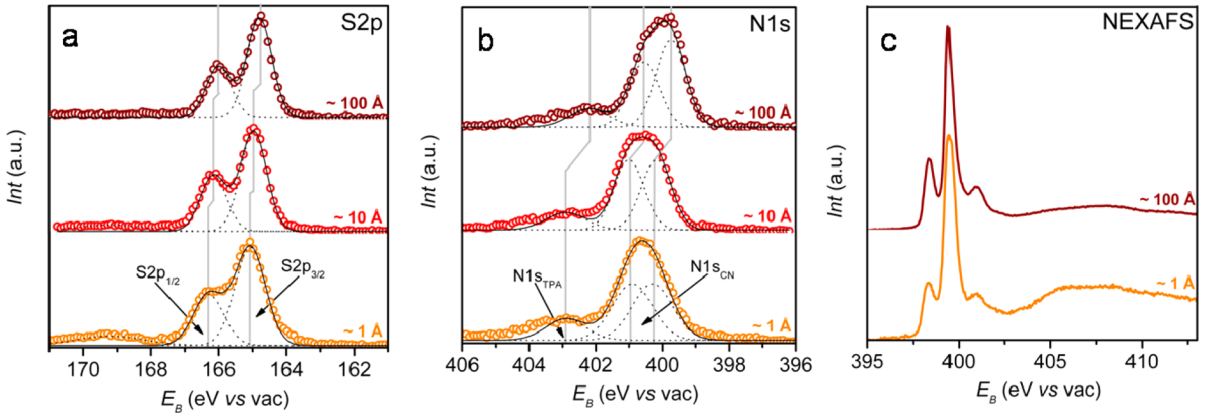

Figure 5. Photo electron spectra of the S2p (a) and N1s (b) signals for dye layers in different thickness domains (indicated in figure). The nitrogen on the triphenylamine ($N1s_{TPA}$) can be distinguished the cyano-nitrogen ($N1s_{CN}$). (c) N1s-NEXAFS spectra for the submonolayer and bulk dye layer of TDCV-TPA on titanium dioxide.

chemical environments of the cis and trans CN-nitrogen atoms. When analyzing the complete N1s spectra, we note that the ratio between the $N1s_{TPA}$ and $N1s_{CN}$ signals vary between 1:5.2 for the submonolayer and 1:6.3 for the multilayer, which agrees rather well with the atomic ratio 1:6. For the submonolayer (~1 Å) and monolayer (~10 Å) the $N1s_{TPA}$ and $N1s_{CN}$ appear shifted to higher E_B by 0.7 and 0.4 eV with respect to the multilayer (~100 Å).

The N1s-NEXAFS spectra of the submonolayer and multilayers of dyes on TiO_2 are shown in Figure 5c. We observe sharp resonances at about 398.4, 399.5, and 401.0 eV, and a broader band between 405 and 415 eV. The spectra are rather similar to N1s NEXAFS spectra previously measured for the smaller dye molecules mentioned above.[39,40] Based on the experiments and calculations made in these references, we can conclude that the three resonances at lower photon energy originate from the CN units while the structures observed at higher photon energies originate from the triphenylamine moiety. In the NEXAFS spectrum for the submonolayer, the resonance peak at 398.4 eV is considerably lower in intensity relative to the peak at 399.5 eV compared to that for the multilayer of dye. The former corresponds to the out-of-plane antibonding C≡N orbital, which overlaps and contributes to the conjugated π-system.[40] The resonance peak at 399.5 eV on the other hand corresponds to the in-plane antibonding C≡N orbital.[40] The difference in intensity for these two peaks indicates differences in the molecular electronic structure related to the CN groups for the monolayer compared to the multilayer of molecules. Also the intensity of the structure at higher photon energies 405−415 eV is different for the monolayer and the multilayer of molecules. This structure is dominated by σ-resonances from the triphenylamine moiety.[30]

UV−Vis and Photoluminescence. In Figure 6a the normalized light harvesting efficiency, LHE (circles), together with the photoluminescence (PL) excitation and emission spectra (solid lines) are compared for different d (indicated in figure). TDCV-TPA dispersed in a PMMA matrix (<1 μmol/g PMMA) was used as a point of reference for TDCV-TPA in a "solid solution" which was found to resemble the solution spectrum of the dye in dichloromethane.[20] The absorption maxima for the $\pi\rightarrow\pi^*$ transition, $E^{\pi\rightarrow\pi^*}_{abs,max}$, and intramolecular charge transfer (ICT), $E^{ICT}_{abs,max}$, transitions as well as the emission maximum, PL_{max}, and the absorption onset, ΔE_{opt}, are summarized in Table 1.

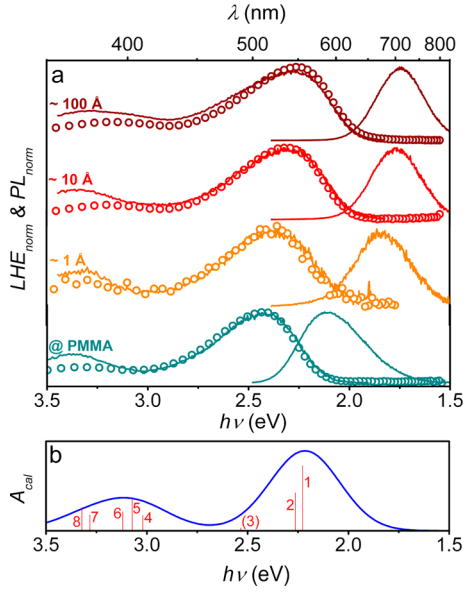

Figure 6. (a) Light harvesting efficiency spectra (circles) and photoluminescence excitation and emission spectra (solid line) of TDCV-TPA films of varying thickness d and in PMMA (indicated in figure). (b) Theoretical absorption spectrum of TDCV-TPA from TD-DFT calculations (assignment in Table 2).

Table 1. Summary of Absorption ($A_{\pi\rightarrow\pi^*}$ and A_{ICT}), Emission Maxima (PL_{max}), and Optical Bandgap ΔE_{0pt} of the Experimental TDCV-TPA Spectra Shown in Figure 6a

	$E^{\pi\rightarrow\pi^*}_{abs,max}$ (eV)	$E^{ICT}_{abs,max}$ (eV)	PL_{max} (eV)	ΔE_{opt} (eV)
@ PMMA	3.37	2.43	2.12	2.12
1 Å film	3.36	2.38	1.84	2.07
10 Å film	3.20	2.30	1.77	2.00
100 Å film	3.18	2.26	1.74	1.98

The absorption band of TDCV-TPA around 380 nm is assigned to a $\pi\rightarrow\pi^*$ transition while the absorption band at around 500 nm is ascribed to an ICT-transition.[20] The theoretical absorption spectrum calculated with time-dependent DFT is shown in Figure 6b. The assignment of the different electronic transitions indicated in the spectrum with numbers can be found in Table 2. The dominating frontier orbitals for the three highest HOMOs and lowest LUMOs that are mainly

dx.doi.org/10.1021/jp302187w | J. Phys. Chem. C 2012, 116, 21148−21156

Table 2. Theoretical Electronic Transitions Determined from Time-Dependent DFT Calculations[a]

transition	ΔE (eV)	λ (nm)	oscillator strength	symmetry	major contributions
1	2.23	556.8	1.02	singlet	HOMO−LUMO (99%)
2	2.26	547.9	0.59	singlet	HOMO−LUMO+1 (99%)
3	2.53	489.4	0.05	singlet	HOMO−LUMO+2 (94%)
4	3.02	410.6	0.24	singlet	HOMO-1−LUMO (99%)
5	3.07	403.6	0.49	singlet	HOMO-1−LUMO +1 (51%)
					HOMO-2−LUMO (49%)
6	3.12	397.4	0.30	singlet	HOMO-2−LUMO +1 (98%)
7	3.28	377.7	0.25	singlet	HOMO-2−LUMO (36%)
					HOMO-1−LUMO +1 (32%)
					HOMO−LUMO+2 (24%)
8	3.32	373.2	0.36	singlet	HOMO-2−LUMO +2 (98%)

[a]The transitions are indicated in Figure 5b.

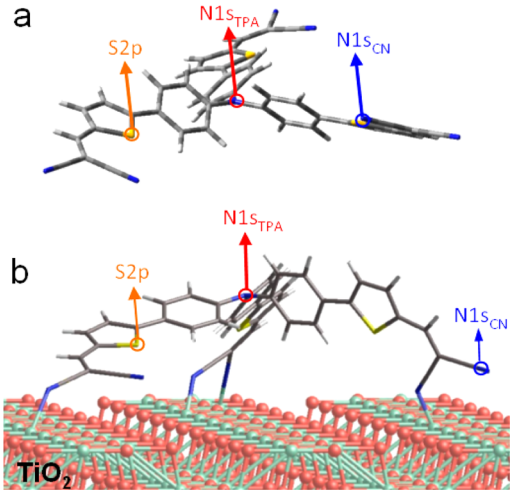

Figure 7. (a) Theoretical molecular conformation of the energetically relaxed TDCV-TPA calculated in the gas phase. (b) Molecular conformer (tripod) that would allow a simultaneous interaction of TDCV-TPA via all three branches with the TiO_2 surface (the (100)-surface is shown for illustration only).

involved in the electronic transitions, are included in Figure 8 for the visualization of the electron density distribution in these molecular orbitals. The electronic transitions below 2.7 eV (Table 2) have the highest oscillator strength and contain excitations involving the HOMO, where the computed electron density distribution is predominantly located on the central triphenylamine unit, and the LUMO and LUMO+1 with electron densities being situated on the peripheral branches of the molecule. The higher energy transitions above 2.7 eV predominantly originate from the HOMO-1 and HOMO-2 and end in the LUMO, LUMO+1, and LUMO+2.

As visualized in the frontier molecular orbitals included in Figure 8, these transitions are of $\pi\rightarrow\pi^*$ character which confirms the previous assignment.[19,20] The shift of the optical transitions in the UV and visible region in a different dielectric environment can be theoretically calculated as described in the Experimental Section. A *blue-shift* of the UV transitions on the order of 0.25 eV and a *red-shift* of the visible transitions in the order of 0.20 eV was obtained an environment corresponding to the dielectric conditions in PMMA. The $\pi\rightarrow\pi^*$ transition in the UV corresponds well with the experimental UV transition measured in PMMA while the theoretical ICT transitions in the visible are more sensitive to an exact description of the environment, as expected.

In comparison to the spectra of TDCV-TPA in PMMA, the LHE spectra of solid films of TDCV-TPA on TiO_2 are broader with a red-shift in the absorption maximum, $E^{ICT}_{abs,max}$ (Table 1), with increasing d. The photoluminescence (PL) appears quite drastically red-shifted for TDCV-TPA films in comparison with the spectrum of the solid solution in PMMA. Because of the ICT nature of the lower energy transition the TDCV-TPA solution spectra is strongly influenced by solvent polarity exhibiting a red-shift of the emission maximum and a profoundly decreased photoluminescence quantum yield Φ_{PL} in more polar sovents.[20]

The PL emission maximum of TDCV-TPA in PMMA is comparable with PL_{max} in toluene solution while the PL_{max} of a submonolayer on glass is shifted by 0.28 eV, which is comparable to the PL_{max} measured in acetone solution.[20] The red-shift of the PL_{max} and decrease in Φ_{PL} (<15% with respect to the PL in PMMA) reflects the different chemical environment upon interaction with the TiO_2 surface and dye−dye interaction in the bulk of the TDCV-TPA film. In addition, this drastic red-shift can be caused by dye-aggregate formation and spectral diffusion. The latter is often observed in materials with a distribution of exciton energy levels when excitons diffuse to lower energy sites from where they emit.[41−43] Investigation into the exact nature of this phenomenon is beyond the scope of this work. The progressive shift and distortion apparent in the ICT band within increasing d can be explained with dye−dye interactions in the aggregated dye layer.

DISCUSSION

According to eq 2, photoinduced charge-transfer at the hetero interface between the small molecular semiconductor TDCV-TPA and TiO_2 depends on the overlap between the dye-excited state and accessible DOS in TiO_2 as well as the electronic coupling. Therefore, the interfacial energetics and molecular interaction of the first layer of TDCV-TPA molecules on TiO_2 largely determines the charge separation efficiency of the whole solar cell device.

Molecular Orientation. TDCV-TPA resembles other triphenylamine-based dyes designed for the sensitization of TiO_2 in DSC.[36,37] However, the dye does not feature functional groups such as carboxylic acids which allows the dye to chemically bind to the TiO_2 surface. Indications for an interaction of TDCV-TPA with TiO_2 via the peripheral CN-groups of the molecule were found in the shifts observed in the N1s PES-signals (Figure 5b) and the NEXAFS spectrum (Figure 6). Moreover, in complementary IR-measurements conducted on TDCV-TPA adsorbed from dilute solution onto mesoporous TiO_2 films (representing low coverage, see Supporting Information), we observed a peak shift and the

dx.doi.org/10.1021/jp302187w | J. Phys. Chem. C 2012, 116, 21148−21156

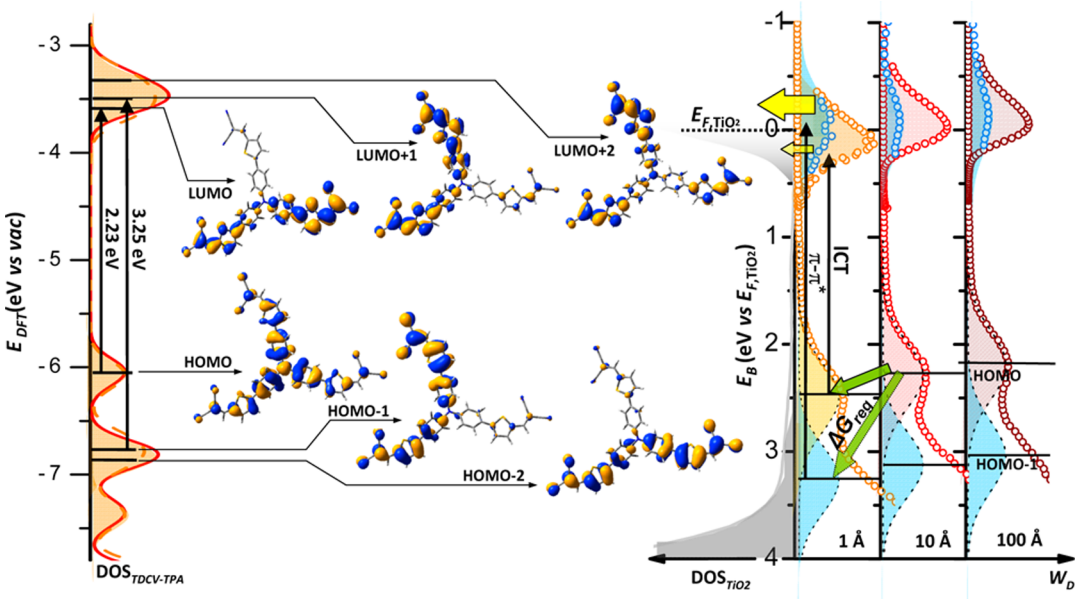

Figure 8. (left) Theoretical density of states for TDCV-TPA. (center) Optically dominating frontier orbitals from DFT calculations showing the electron density distribution of the HOMOs and LUMOs. (right) Energy level diagram derived from the Gaussian fits to PES measurements with respect to the Fermi-level E_F in TiO_2 and extrapolated optical transitions for dye layers in different thickness domains (indicated in graph).

presence of a asymmetric broadening in the cyano-group vibration to higher energy when compared to the IR-spectrum measured on a solid film. Again, this may be interpreted as indication for an associative interaction between the cyano-groups and the TiO_2 surface.

The indications of an interaction between the cyano groups in TDCV-TPA with the TiO_2 surface lead us to suggest that the dye adopts a tripod-like conformation, in which the molecule interacts with the TiO_2 surface via several or all CN-groups simultaneously (Figure 7b). In DFT-calculations the tripod-conformer is 0.3 eV higher in energy compared to the fully energy relaxed conformation (Figure 7a). Calculations of the interaction between a single CN-group of TDCV-TPA with a small section of the crystalline anatase TiO_2 surface gave an interaction energy of 0.3−0.4 eV after relaxation and counter-poise correction. The absolute values depend on the immediate surrounding of the Ti atom which is different for the anatase (100) and (101) surface. These values are comparable to DFT calculations carried out on the interaction between acetonitrile molecules and the anatase (101) TiO_2 surface.[44,45] For a full monolayer coverage of acetonitrile on the anatase (101) TiO_2 surface, the interaction energy per acetonitrile molecule was found to be between 0.2 and 0.4 eV. For single molecules the interaction energies were calculated to be 0.6 to 0.8 eV. We conclude that the energy gain due to the interaction of one out of the six CN-groups of TDCV-TPA with the TiO_2 surface can already balance out the energy necessary for the molecule to adopt a tripod-like conformation.

In Figure 8, the electron density distribution in the three highest occupied molecular orbitals (HOMOs) and lowest unoccupied molecular orbitals (LUMOs) calculated for TDCV-TPA in the gas-phase are shown. In the excited state, the electron density is located on the branches of the dye molecule and is increasingly shifted toward the peripheral dicyano-vinyl groups. The electron density distribution for the tripod-conformation (not shown) gave a similar picture of electron density being shoved toward the branches of the molecule.

Considering this redistribution of electron-density onto the CN-groups and a preferential interaction of the molecule with TiO_2 via those groups suggests a beneficial electronic coupling for interfacial electron transfer. Upon interaction between TDCV-TPA and TiO_2 electron density of the dye-LUMOs can possibly be redistributed onto energetically similar 3d orbitals constituting the TiO_2 conduction band. In the case that TDCV-TPA coordinates with only one branch to TiO_2 the η_{CT} should be lower compared to coordination with two or three branches as, statistically, the electron-density might shift away from the surface upon excitation of the molecule.

Energy Level Alignment. Previously, we derived a simple energy level diagram for the TDCV-TPA/TiO_2 heterojunction estimating the HOMO for TDCV-TPA from the oxidation potential determined by cyclic voltammetry in solution.[11] For comparison, we carried out electrochemical differential pulse voltammetry of TDCV-TPA in solution and on solid films on FTO (Supporting Information). From these measurements, the oxidation potential for a TDCV-TPA film was determined to be 1.26 V vs normal hydrogen electrode (NHE) which corresponds to 5.86 eV vs vacuum using the relation $E_{F,redox}$ [eV] = 4.6 ± 0.1 − eV_{redox} [V].[12] We recently determined the flatband potential for spray-pyrolyzed TiO_2 on FTO substrates to −0.5 vs NHE which can be approximated as the E_{F,TiO_2} and corresponds to 4.1 eV vs vacuum.[35] Based on this conversion, the oxidation potential measured in solution is comparable to the theoretical HOMO calculated with DFT (Figure 4b), but at least 0.5 eV higher than the HOMO measured by PES (6.35 eV vs vac for a dye-multilayer).

The uncertainty inherent in the conversion factors relating redox-chemical, theoretical, and photoelectron spectroscopic energy scales makes this comparison difficult. Deviations between oxidation potentials measured electrochemically and HOMOs measured by PES are ascribed to the impact of solvation and polarization effects in electrochemical measurements[46] and/or changes in the Fermi level due to electron

transfer induced by the adsorption of the molecular compound to the substrate.

The shift of the HOMO levels observed for the dye layer closest to the TiO_2 surface to higher binding energies with respect to the dye molecules in the bulk (Figure 4a) indicates that adsorption induces a change in the molecular energy level alignment. The downward shift of the HOMO at the junction is advantageous in terms of separating interfacial geminate electron hole pairs via hole transfer to the dye layers adjacent to the interfacial dye layer. These results illustrate that the energy level alignment at an organic/inorganic solid state hetero interface may be obtained with experimental techniques that allow the direct investigation of this interface.

A diagram was derived from the PES (Figure 4a) and UV−vis (Figure 6a) measurements conducted on dye layers in different thickness regimes, see Figure 8 (right-hand side). To estimate the energy level alignment of the excited state of TDCV-TPA with respect to the E_F in TiO_2, we superimposed the experimental absorption spectra on top of the HOMO energy levels measured with PES.

From theoretical calculations (Figure 6b and Table 2) we found that the optical transitions above ∼2.8 eV ($\pi \rightarrow \pi^*$) originate predominantly from the HOMO-1 and HOMO-2 and the lower energy (ICT) transitions, originate predominantly from the HOMO of TDCV-TPA. Taking this difference in character into account we superimposed the energy distribution of the two different experimentally observed UV−vis features on the estimated HOMO and HOMO-1 peak positions in PES spectra.

The TiO_2 valence band onset of the spray-pyrolyzed TiO_2 substrates was measured to be about 3.2 eV below the E_F of TiO_2 by PES (Supporting Information) which is close to the optical band gap (3.4 eV) measured for these substrates with UV−visible spectroscopy.[35] The conduction band edge of TiO_2 is thus close to the E_{F,TiO_2}. The conduction band DOS is not expected to seize abruptly but exhibits a tail of electronic states below the conduction band edge.[47]

The excited states of TDCV-TPA are just at the edge of the E_F in TiO_2. From the derived energy level diagram (Figure 8) it seems that there a small thermodynamic advantage for electron injection from the higher energy transitions. As the density of states increase steeply above the conduction band edge electron injection for higher energy transitions can become more favorable.

In Figure 8 (left side), we also included the theoretical DOS for the energy-optimized (Figure 7a) and the tripod-conformer (Figure 7b), based on a similar procedure as used for the experimental results. Dye excitation results in states with minor differences in driving force for electron injection. On the right-hand side, a direct comparison is made with the DOS in TiO_2 and fits of the HOMO, HOMO-1 and HOMO-2 derived from PES measurements (Figure 4a) for dye layers in different thickness domains.

A wavelength dependent IQE, as we observed at the heterojunction investigated herein, can in some cases be rationalized invoking differences in the driving force for electron injection from higher excited electronic and vibronic transitions.[24] Injection from "hot" excited states has been observed in DSC-devices[23,48] and also plays a role in overcoming attractive forces in charge-transfer complexes formed at organic heterojunctions.[10]

Differentiating between the higher energy and lower energy electronic transitions we do not find a clear energetic advantage for electron transfer to TiO_2 conduction band states following excitation of higher energy ($\pi-\pi^*$) electronic transitions. The energetic alignment of the excited states with respect to the E_{F,TiO_2} in the derived energy level diagram (Figure 8, right) does not allow a rationalization of the observed excitation-energy dependent IQE due to a higher driving force for electron injection for the $\pi-\pi^*$ transition.

We note that holes created following these higher energy transitions might be regenerated more efficiently via hole transfer to a consecutive dye molecule, compared to holes created following ICT-transitions, originating from the HOMO. In accordance with the charge separation process in organic solar cell devices,[10] factors promoting the special separation of interfacial electrons and holes also affect the charge separation efficiency in the type of HSC investigated here.

CONCLUSION

At the investigated hetero interface between the small-molecular semiconductor TDCV-TPA and titanium dioxide, an excitation energy dependent internal quantum efficiency, IQE, and stronger photoluminescence quenching at higher excitation energy were observed. This implies a more efficient separation for the higher energy $\pi-\pi^*$ transition in TDCV-TPA at the investigated organic−inorganic heterojunction.

PES and IR-measurements indicated that TDCV-TPA interacts with TiO_2 via its peripheral cyano-groups. We propose that dye molecules adjacent to the TiO_2 surface attain a tripod geometry. This will result in a more favorable electronic coupling for photoinduced electron transfer from TDCV-TPA to TiO_2.

Using experimental and computational results, a detailed energy level diagram was constructed differentiating between the character of the higher energy and lower energy electronic transitions in TDCV-TPA. This diagram reveals that all excited states are very close in energy to the conduction band edge of TiO_2. Higher energy transitions result in only marginally larger driving force for interfacial electron transfer.

Another factor affecting the interfacial charge separation is the regeneration of holes created at the interface. PES measurements indicated that energy levels of the dye layer closest to the TiO_2 surface are shifted to higher binding energy compared to energy levels measured for molecules in the bulk of the dye layer. This molecular band-bending at the heterojunction is beneficial for the separation of the geminate electron hole pairs created at this interface. Furthermore, holes created following higher energy ($\pi-\pi^*$) transitions are likely more efficiently regenerated.

ASSOCIATED CONTENT

Supporting Information

Electrochemical differential pulse voltammetry measurements of TDCV-TPA in solution and as a solid film. IR spectra analyzing the TDCV-TPA/TiO_2 interaction. This material is available free of charge via the Internet at http://pubs.acs.org.

AUTHOR INFORMATION

Corresponding Author

*Telephone: +46-(0)18-471 3303. Fax: +46-(0)18-471 3633. E-mail: Gerrit.Boschloo@kemi.uu.se.

Notes

The authors declare no competing financial interest.

■ ACKNOWLEDGMENTS

This project was funded by the Swedish Research Council (Vetenskapsrådet), the Swedish Energy Agency and the STandUP for Energy program. E.M.J.J. thanks the Göran Gustafsson stiftelse for financial support. J.D.R.-M. is supported by the National Science Foundation Graduate Research Fellowship under Grant No. DGE-0646086. E.L.U. thanks Burkhard Zietz from the Department of Chemistry, Uppsala University for interesting discussions about optical transitions in aggregated dye layers. We thank the staff at MAX-lab for competent and friendly assistance.

■ REFERENCES

(1) Bouclé, J.; Ackermann, J. *Polym. Int.* **2012**, *61*, 355−373.
(2) Bouclé, J.; Ravirajan, P.; Nelson, J. *J. Mater. Chem.* **2007**, *17*, 3141.
(3) Arici, E.; Sariciftci, N. S.; Meissner, D. *Encycl. Nanosci. Nanotechnol.* **2004**, *3*, 929.
(4) Günes, S.; Sariciftci, N. S. *Inorg. Chim. Acta* **2008**, *361*, 581.
(5) McGehee, M. D. *MRS Bull.* **2009**, *34*, 95.
(6) Gregg, B. A. *J. Phys. Chem. B* **2003**, *107*, 4688.
(7) Gregg, B. A. *MRS Bull.* **2005**, *30*, 20.
(8) Ardo, S.; Meyer, G. J. *Chem. Soc. Rev.* **2009**, *38*, 115.
(9) Gerischer, H.; Willig, F.; Schäfer, F.; Gerischer, H.; Willig, F.; Meier, H.; Jahnke, H.; Schönborn, M.; Zimmermann, G. Reaction of excited dye molecules at electrodes. In *Physical and Chemical Applications of Dyestuffs*; Springer: Berlin/Heidelberg, 1976; Vol. *61*, p 31.
(10) Clarke, T. M.; Durrant, J. R. *Chem. Rev.* **2010**, *110*, 6736−6767.
(11) Unger, E. L.; Ripaud, E.; Leriche, P.; Cravino, A.; Roncali, J.; Johansson, E. M. J.; Hagfeldt, A.; Boschloo, G. *J. Phys. Chem. C* **2010**, *114*, 11659.
(12) Hagfeldt, A.; Boschloo, G.; Sun, L.; Kloo, L.; Pettersson, H. *Chem. Rev.* **2010**, *110*, 6595.
(13) Gowrishankar, V.; Hardin, B. E.; McGehee, M. D. TiO_2 Template/Polymer Solar Cells. In *Organic Photovoltaics: Materials, Device Physics and Manufacturing Technologies*; Brabec, C. J., Dyakonov, V., Scherf, U., Eds.; WILEY-VCH Verlag GmbH: Weinheim, 2008; p 329.
(14) Daoud, W. A.; Turner, M. L. *React. Funct. Polym.* **2006**, *66*, 13.
(15) Ravirajan, P.; Bradley, D. D. C.; Nelson, J.; Haque, S. A.; Durrant, J. R.; Smit, H. J. P.; Kroon, J. M. *Appl. Phys. Lett.* **2005**, *86*, 143101.
(16) Goh, C.; Scully, S. R.; McGehee, M. D. *J. Appl. Phys.* **2007**, *101*, 114503.
(17) Lira-Cantu, M.; Krebs, F. C. *Sol. Energy Mater. Sol. Cells* **2006**, *90*, 2076.
(18) Savenije, T. J.; Warman, J. M.; Goossens, A. *Chem. Phys. Lett.* **1998**, *287*, 148.
(19) Cravino, A.; Roquet, S.; Leriche, P.; Alévêque, O.; Frère, P.; Roncali, J. *Chem. Commun.* **2006**, 1416.
(20) Roquet, S.; Cravino, A.; Leriche, P.; Alévêque, O.; Frère, P.; Roncali, J. *J. Am. Chem. Soc.* **2006**, *128*, 3459.
(21) Davis, R. J.; Lloyd, M. T.; Ferreira, S. R.; Bruzek, M. J.; Watkins, S. E.; Lindell, L.; Sehati, P.; Fahlman, M.; Anthony, J. E.; Hsu, J. W. P. *J. Mater. Chem.* **2011**, *21*, 1721.
(22) Cappel, U. B.; Plogmaker, S.; Johansson, E. M. J.; Hagfeldt, A.; Boschloo, G.; Rensmo, H. *Phys. Chem. Chem. Phys.* **2011**, *13*, 14767.
(23) Ferrere, S.; Gregg, B. A. *J. Am. Chem. Soc.* **1998**, *120*, 843.
(24) Nevin, W. A.; Chamberlain, G. A. J. *Appl. Phys. Chem.* **1991**, *69*, 4324.
(25) Braun, S.; Osikowicz, W.; Wang, Y.; Salaneck, W. R. *Org. Electronics* **2007**, *8*, 14.
(26) Johansson, E. M. J.; Hedlund, M.; Siegbahn, H.; Rensmo, H. *J. Phys. Chem. B* **2005**, *109*, 22256.
(27) Johansson, E. M. J.; Karlsson, P. G.; Hedlund, M.; Ryan, D.; Siegbahn, H.; Rensmo, H. k. *Chem. Mater.* **2007**, *19*, 2071.
(28) Johansson, E. M. J.; Schölin, R.; Siegbahn, H.; Hagfeldt, A.; Rensmo, H. *Chem. Phys. Lett.* **2011**, *515*, 146.
(29) Ishii, H.; Sugiyama, K.; Ito, E.; Seki, K. *Adv. Mater.* **1999**, *11*, 605.
(30) Johansson, E. M. J.; Odelius, M.; Karlsson, P. G.; Siegbahn, H.; Sandell, A.; Rensmo, H. *J. Chem. Phys.* **2008**, *128*, 184709.
(31) Bröker, B.; Hofmann, O. T.; Rangger, G. M.; Frank, P.; Blum, R. P.; Rieger, R.; Venema, L.; Vollmer, A.; Müllen, K.; Rabe, J. P.; et al. *Phys. Rev. Lett.* **2010**, *104*, 246805.
(32) Bässler, M.; Forsell, J. O.; Björneholm, O.; Feifel, R.; Jurvansuu, M.; Aksela, S.; Sundin, S.; Sorensen, S. L.; Nyholm, R.; Ausmees, A.; et al. *J. Electron Spectrosc. Relat. Phenom.* **1999**, *101*−*103*, 953.
(33) Svensson, S.; Forsell, J. O.; Siegbahn, H.; Ausmees, A.; Bray, G.; Södergren, S.; Sundin, S.; Osborne, S. J.; Aksela, S.; Nommiste, E.; et al. *Rev. Sci. Instrum.* **1996**, *67*, 2149.
(34) Schniepp, H. C.; Saville, D. A.; Aksay, I. A. *J. Am. Chem. Soc.* **2006**, *128*, 12378.
(35) Unger, E. L.; Spadavecchia, F.; Nonomura, K.; Palmgren, P.; Cappelletti, G.; Johansson, E. M. J.; Hagfeldt, A.; Boschloo, G. Submitted.
(36) Hagberg, D. P.; Yum, J.-H.; Lee, H.; De Angelis, F.; Marinado, T.; Karlsson, K. M.; Humphry-Baker, R.; Sun, L.; Hagfeldt, A.; Grätzel, M.; et al. *J. Am. Chem. Soc.* **2008**, *130*, 6259.
(37) Hagberg, D. P.; Marinado, T.; Karlsson, K. M.; Nonomura, K.; Qin, P.; Boschloo, G.; Brinck, T.; Hagfeldt, A.; Sun, L. *J. Org. Chem.* **2007**, *72*, 9550.
(38) Hahlin, M.; Johansson, E. M. J.; Plogmaker, S.; Odelius, M.; Hagberg, D. P.; Sun, L.; Siegbahn, H.; Rensmo, H. *Phys. Chem. Chem. Phys.* **2010**, *12*, 1507.
(39) Johansson, E. M. J.; Edvinsson, T.; Odelius, M.; Hagberg, D. P.; Sun, L.; Hagfeldt, A.; Siegbahn, H.; Rensmo, H. *J. Phys. Chem. C* **2007**, *111*, 8580.
(40) Hahlin, M.; Odelius, M.; Magnuson, M.; Johansson, E. M. J.; Plogmaker, S.; Hagberg, D. P.; Sun, L.; Siegbahn, H.; Rensmo, H. *Phys. Chem. Chem. Phys.* **2011**, *13*, 3534.
(41) Gregg, B. A.; Sprague, J.; Peterson, M. W. *J. Phys. Chem. B* **1997**, *101*, 5362.
(42) Harrison, M. G.; Grüner, J.; Spencer, G. C. W. *Phys. Rev. B* **1997**, *55*, 7831.
(43) Karpicz, R.; Puzinas, S.; Krotkus, S.; Kazlauskas, K.; Jursenas, S.; Grazulevicius, J. V.; Grigalevicius, S.; Gulbinas, V. *J. Chem. Phys.* **2011**, *134*, 204508.
(44) Schiffmann, F.; Hutter, J.; VandeVondele, J. *J. Phys.: Condens. Matter* **2008**, 20.
(45) Mosconi, E.; Selloni, A.; de Angelis, F. *J. Phys. Chem. C* **2012**, *116*, 5932−5940.
(46) Andrade, B. W.; Datta, S.; Forrest, S. R.; Djurovich, P.; Polikarpov, E.; Thompson, M. E. *Org. Electron.* **2005**, *6*, 11.
(47) Bisquert, J.; Fabregat-Santiago, F.; Mora-Seró, I.; Garcia-Belmonte, G.; Barea, E. M.; Palomares, E. *Inorg. Chim. Acta* **2008**, *361*, 684.
(48) Benkö, G.; Kallioinen, J.; Korppi-Tommola, J. E. I.; Yartsev, A. P.; Sundström, V. *J. Am. Chem. Soc.* **2001**, *124*, 489.